CHAPTER IV

RESULTS AND DISCUSSION

4.1 The Sensitivity of Input Variables

The model for thinning of outlet feeders was developed by many researchers (Johari, 1994; and Lang, 2000) for a better understanding and characterizing the thinning phenomena of outlet feeders. There are many variables in the model affecting the thinning of feeders. Table 4.1 shows the effect of such variables on the corrosion rate predicted by the model for the S08 outlet feeder at a pH of 10.2. From observations, it was found that the corrosion rate of S08 is about 110 μm/yr with an oxide layer thickness of 0.8 μ m. The conditions of base case for S08 are presented in appendix A.

From Table 4.1, it was found that the magnetite solubility has a small effect on corrosion rate. The activation energy of the Fe to Fe^{2+} reaction on the corrosion rate significantly. If this free energy of activation was low, the metal could be converted into ferrous ions more easily and the corrosion rate was significantly increased. If the free energy of activation for converting ferrous ions into magnetite was reduced, the conversion of the irons to magnetite increased and the oxide layer became thicker reducing the corrosion rate high. From Eq.2.7, it is found that local solubility of magnetite varied with H$_2$ concentration to the 1/3 power according to Eq.4.1.

$$[C_{eq}] \propto [H_2]^{1/3} \tag{4.1}$$

where [C$_{eq}$] = magnetite solubility

[H$_2$] = H$_2$ concentration.

Table 4.1 The effect of input variables.

Input	Corrosion Rate (μm/yr)
Base case	110
Inlet section solubility (double)	117
Inlet section solubility (half)	107
Outlet section solubility (double)	110
Outlet section solubility (half)	107
The difference between inlet section solubility and outlet section solubility (double)	109
The difference between inlet section solubility and outlet section solubility (half)	109
Free energy of activation for $Fe=Fe^{2+}+2e^-$ (double)	0
Free energy of activation for $Fe=Fe^{2+}+2e^-$ (half)	659
Free energy of activation for $FeOH=Fe_3O_4$ (double)	101
Free energy of activation for $FeOH=Fe_3O_4$ (half)	104
Free energy of activation for $Fe^{2+}=Fe_3O_4$ (double)	104
Free energy of activation for $Fe^{2+}=Fe_3O_4$ (half)	29
Free energy of activation for $H^+=H_2$ (double)	27
Free energy of activation for $H^+=H_2$ (half)	112
Outlet inner oxide porosity (double)	140
Outlet inner oxide porosity (half)	72
Outlet inner oxide spalling Constant (double)	73
Outlet inner oxide spalling Constant (half)	149
Dissolution rate constant (double)	139
Dissolution rate constant (half)	75

If hydrogen evolution was reduced the magnetite solubility was decreased. Therefore, the driving force for dissolution was reduced and the corrosion rate was decreased as illustrated in Table 4.1. These activation energies affect the potential which further influences the local solubility.

Porosity is a property of the oxide that affected species diffusion through oxide layer. Porosity enhances diffusion both inwards and outwards of species transferred. A high porosity gives a high corrosion rate, so corrosion rate increased with porosity. Therefore, corrosion rate of feeder S08 increased from 110 μm/yr to 140 μm/yr when porosity was double increased (Table 4.1).

Spalling constant determines spalling time as mentioned in Eq.3.40 and 3.41. A high spalling constant increases spalling time and reduces the rate of particles shearing of from the surface. This causes a decrease in corrosion rate. Corrosion rate of feeder named S08 reduced from 110 μm/yr to 73 μm/yr (Table 4.1).

Dissolution is one of the important mechanisms of corrosion. It depends on the dissolution rate constant and the difference in concentration at the surface and the magnetite solubility. The dissolution rate constant represents the ability of magnetite to dissolve into the solution. The value of this constant depends on temperature and pH and was discussed in section 3.2.7.

4.2 Application of the Model to the Wire Probe

Data have been obtained on wire probes in the FAC loop at the University of New Brunswick. One of the controlled variables studied in the test loop was a pH value. The results from experiments are shown in Table 4.2. The dimensions of wire probe and flow condition are shown in Table 4.3.

Table 4.2 The corrosion rate of wire probe from the experiment.

pH	Corrosion rate (μm/yr)
9.8	12.5
10.4	41.5
11.0	245
11.4	660
11.55	770

Table 4.3 Dimension of wire probe and flow condition.

Inner diameter (cm)	0.316
Outer diameter (cm)	0.13
Hydraulic diameter (cm)	0.186
Length of node1 (cm)	2.3
Length of node2 (cm)	2.7
Coolant velocity (cm/s)	1300
Inlet temperature (°C)	265
Outlet temperature (°C)	310

From Table 4.2, it is found that corrosion rate of feeder pipes increased with pH value. It may be caused by the increase in hydroxyl group that can react with the metal, so corrosion rate increased.

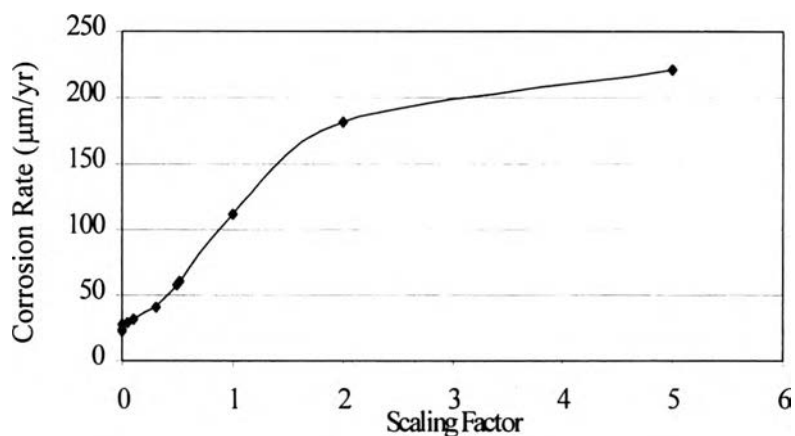### 4.2.1 The Effect of Dissolution Rate Constant

There is a hypothesis that the dissolution rate constant varies with pH. The only data available for magnetite dissolution is at a pH of 10.2 (Balakrishnan, 1977). This data was used with magnetite solubility values

(Tremaine and Leblanc, 1980) to obtain the dissolution rate constant (kd) at a pH of 10.2 by using Eq.3.35. The calculation is illustrated in Appendix D.

A scaling factor (SF) was used for kd at various pH values based on the dissolution rate constant at a pH of 10.2 to obtain the corrosion rate at other pH values. The results from this study is shown in Table 4.4.

Table 4.4 The scaling factor for kd at each pH and predicted corrosion rate of wire probe.

pH	Scaling factor for kd	Predicted corrosion rate (μ m/yr)
9.8	0.00015	12.54
10.4	0.31	41.33

Figure 4.1 Effect of dissolution rate constant in terms of scaling factor on corrosion rate of wire probe at a pH of 10.4.

From Figure 4.1, corrosion rate increases with scaling factor for dissolution rate constant (k$_d$). Dissolution of oxide layer causes decrease in the oxide thickness, so the protective oxide for the metal reduces.
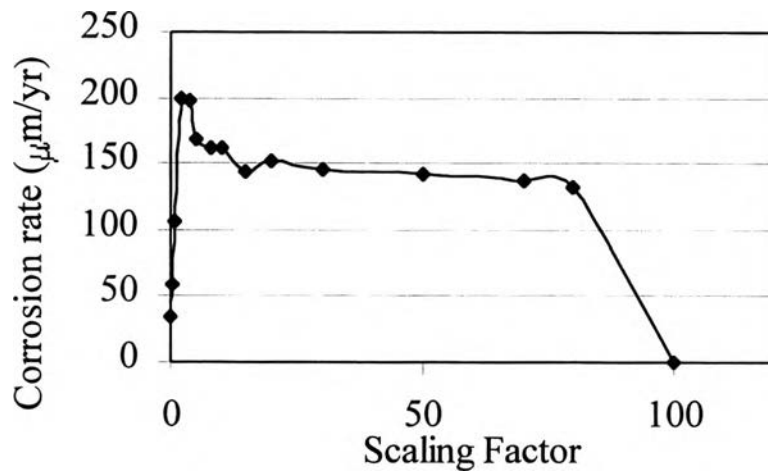
Figure 4.2 Effect of dissolution rate constant in terms of scaling factor on corrosion rate of wire probe at a pH of 11.4.

At high pH, corrosion rate from the experiment (Table 4.2) is high and the value of dissolution rate constant is supposed to be high. From Figure 4.2, a scaling factor for dissolution rate constant which give corrosion rate corresponding with the experiment cannot be determined for high pH. Apparently as the high dissolution rate constant increased the solution becomes saturated and the reaction reverses. A thick oxide layer protects the metal surface from corrosion. Figure 4.1, indicates the corrosion rate increases rapidly with an increase in dissolution rate constant initially followed by a reduction in the rate of increase.
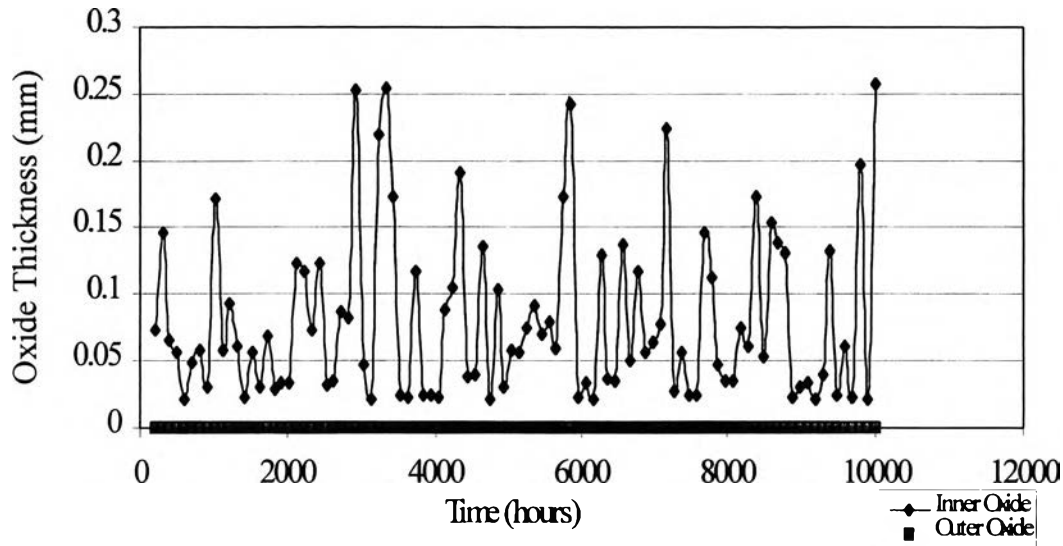
Figures 4.3 to 4.5 present the oxide layer thickness profile at various dissolution rate constants by using scaling factor for dissolution rate at pH of 10.2.
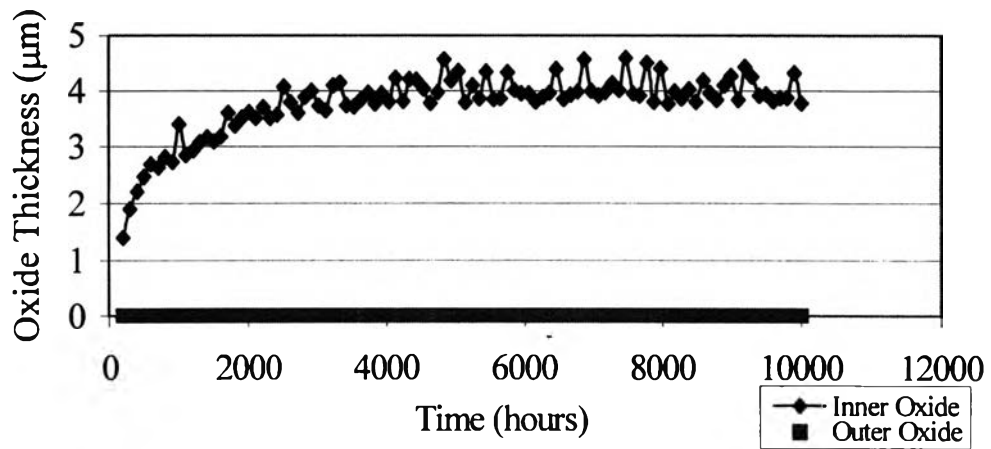
Figure 4.3 Oxide thickness profile with scaling factor 0.5 for kd at pH of 10.2.
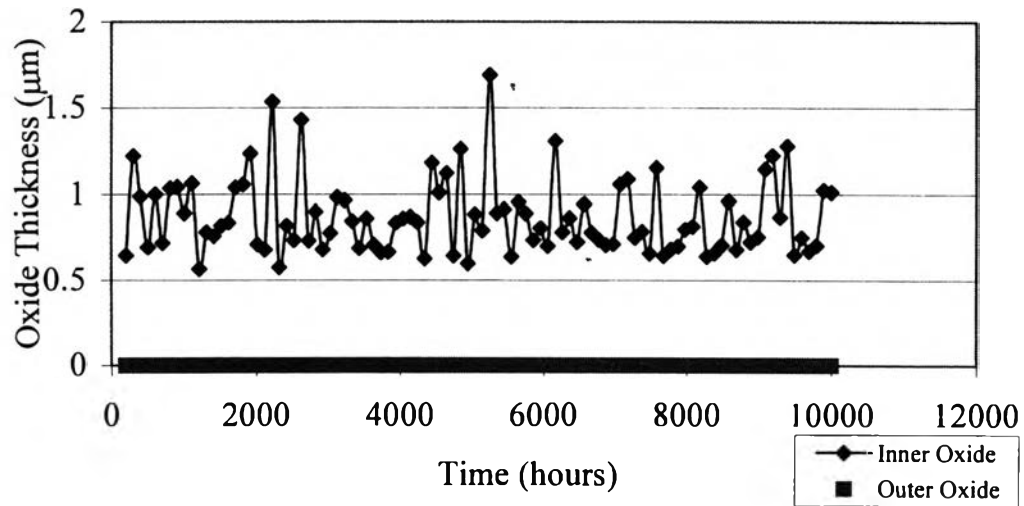
Figure 4.4 Oxide thickness profile with scaling factor 1.0 for k_d at pH of 10.2.

Figure 4.5 Oxide thickness profile with scaling factor 5 for k_d at pH of 10.2.

Figure 4.3, indicates the oxide thickness increases with time and achieves a constant value at longer exposure times. Oxide layer stabilized at about 4 μm, for this case. A high dissolution rate increases magnetite going into solution and yields a thin oxide layer, as Figure 4.4 and Figure 4.5.

4.2.2 The Effect of Free Energy of Activation for Corrosion Reaction

In this study, the values of dissolution rate constant at various pH values were determined by interpolation and extrapolation from Figure 4.6. Figure 4.6, this available dissolution rate constant was based on Balakrishnan's work(1977) and Tremaine and Leblanc's solubilities(1980). The effect of free energy of activation for the corrosion reaction($\Delta G^{\neq}_1$) was varied to obtain a corrosion rate corresponding to experimental data, Table 4.2.
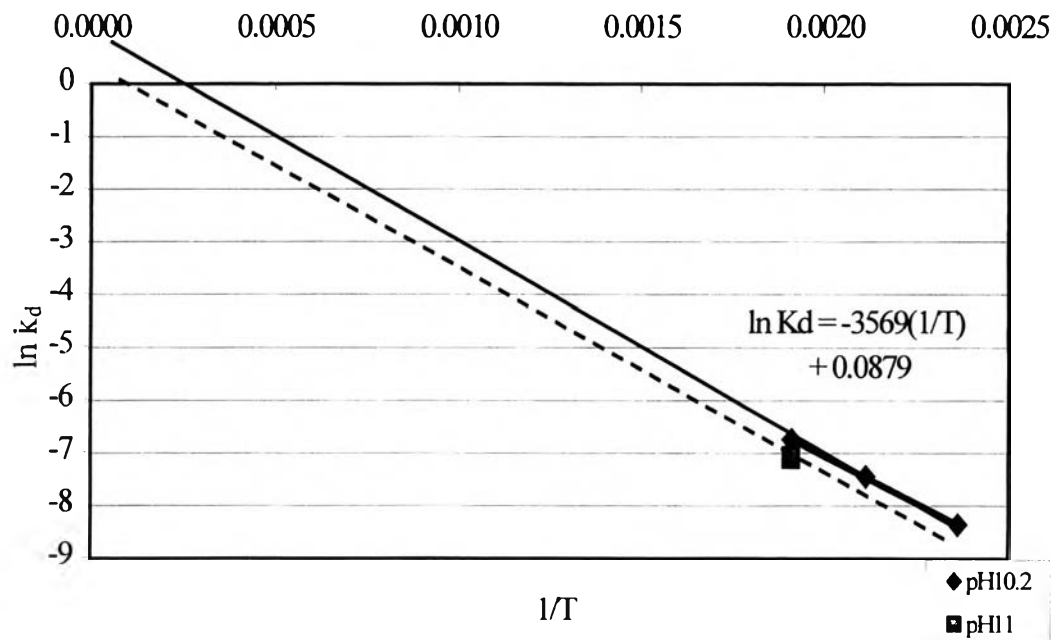
Figure 4.6 Dissolution rate constant at pH10.2 and one datum at pH11.

Assuming the slope of the curve for each pH is the same, the slope of the curve is activation energy for the dissolution reaction. The expressions for dissolution rate constant at pH of 9.8, 10.4, 11, 11.4, and 11.55 are shown in Eqs.4.2, 4.3, 4.4 4.5 and 4.6, respectively.

At pH9.8; $\qquad \ln k_d = -3569/T + 0.2569$ $\qquad$ (4.2)

At pH10.4; $\qquad \ln k_d = -3569/T + 0.0035$ $\qquad$ (4.3)

At pH11; $\qquad \ln k_d = -3569/T - 0.2497$ $\qquad$ (4.4)

At pH11.4; $\qquad \ln k_d = -3569/T - 0.4185$ $\qquad$ (4.5)

At pH11.55; $\qquad \ln k_d = -3569/T - 0.4818$ $\qquad$ (4.6)

Table 4.5 The scaling factor for k_d at each pH and predicted corrosion rate of wire probe.

pH	Scaling factor for $\Delta G^{\neq}_1$	Predicted corrosion rate (μ m/yr)
9.8	1.1015	11.1
11	0.8675	244.73
11.4	0.78	663.13

The relation of free energy of activation and corrosion rate is illustrated in Figure 4.7.
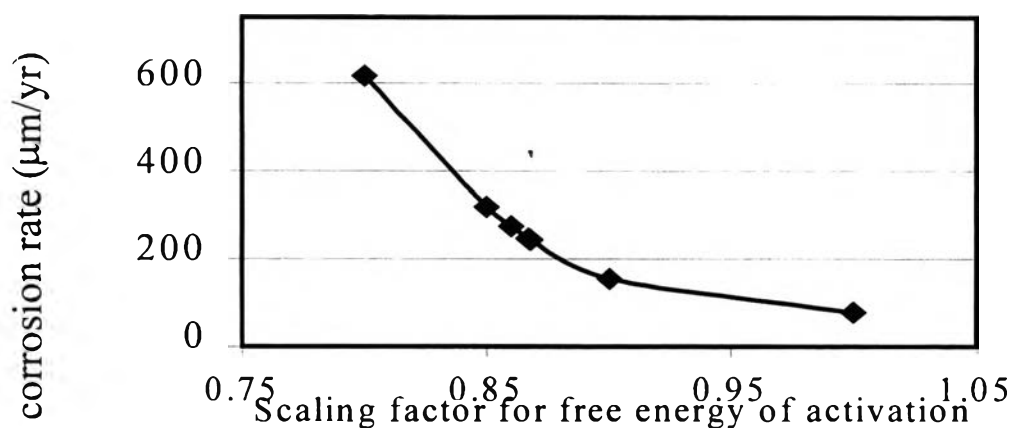
**Figure 4.7** The relation of free energy of activation and corrosion rate at pH of 11.

It is shown that the corrosion rate decreases as the free energy of activation increases. If the activation energy is low, it is easy for the reaction to take place, therefore, the corrosion reaction rate increases.

Figures 4.8 to 4.10 show the change in the oxide layer thickness with time for various values of $\Delta G^{\neq}_1$. When scaling factor for $\Delta G^{\neq}_1$ is 0.8, the oxide layer increased in thickness steadily to about 680 μm/yr at

10000 hours. This result is different from those at scaling factor for $\Delta G^{\neq}_{I}$ of 1 and 1.1, Figures 4.9 and 4.10. The oxide thickness was 2.4 μm and 0.6 μm at scaling factors of $\Delta G^{\neq}_{I}$ 1 and 1.1, respectively.
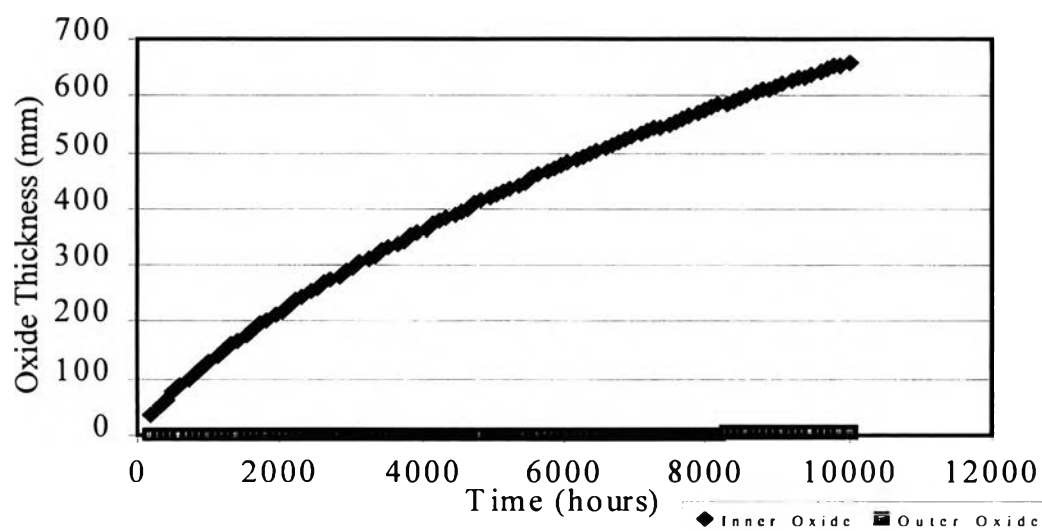
Figure 4.8 The oxide thickness profile within 10000 exposure hours with scaling factor for $\Delta G^{\neq}_{I}$ is 0.8.
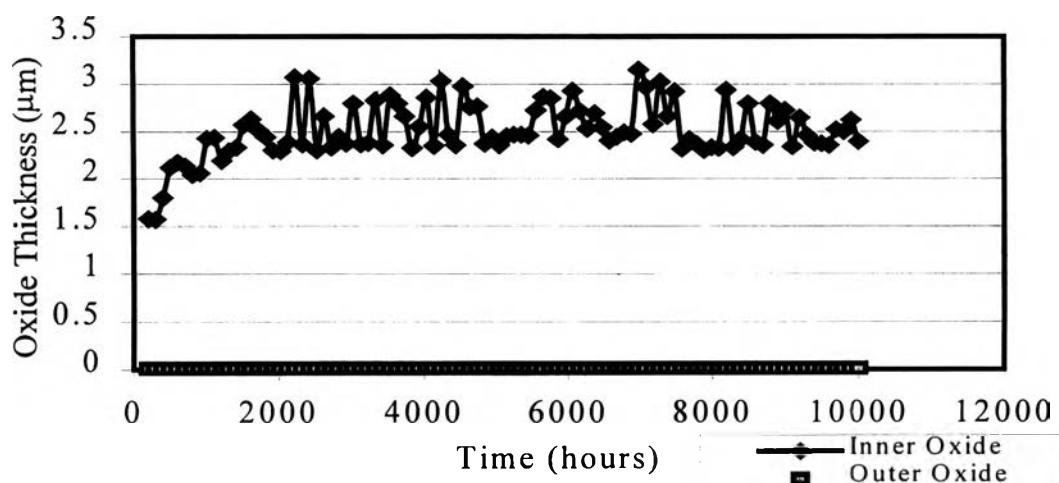
Figure 4.9 The oxide thickness profile within 10000 exposure hours with scaling factor for $\Delta G^{\neq}_{I}$ is 1.
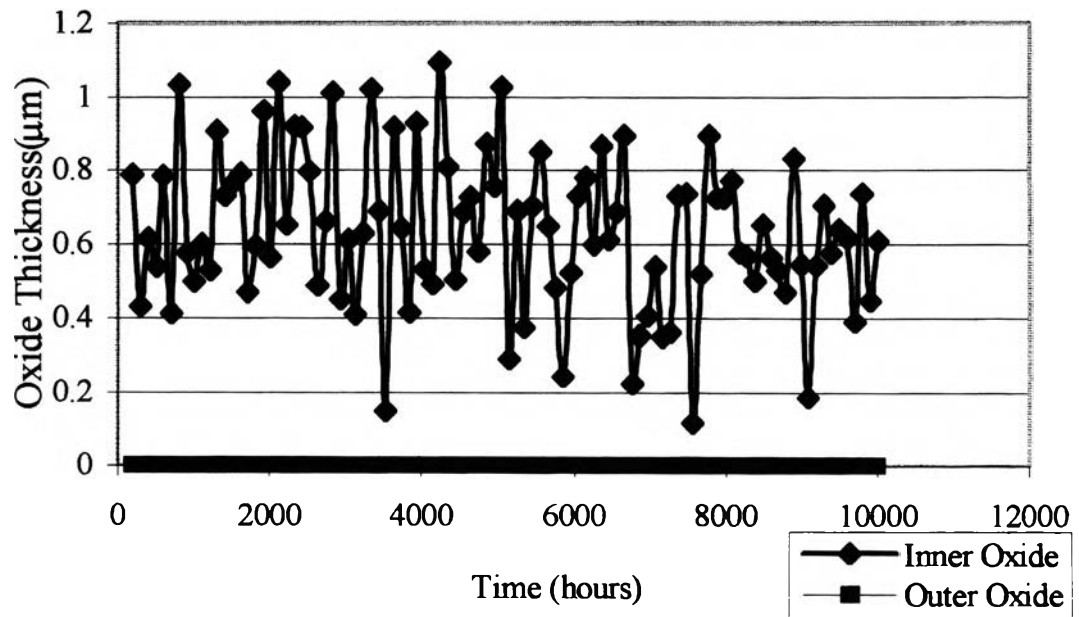
Figure 4.10 The oxide thickness profile within 10000 exposure hours with scaling factor for $\Delta G^{\neq}_1$ is 1.1.

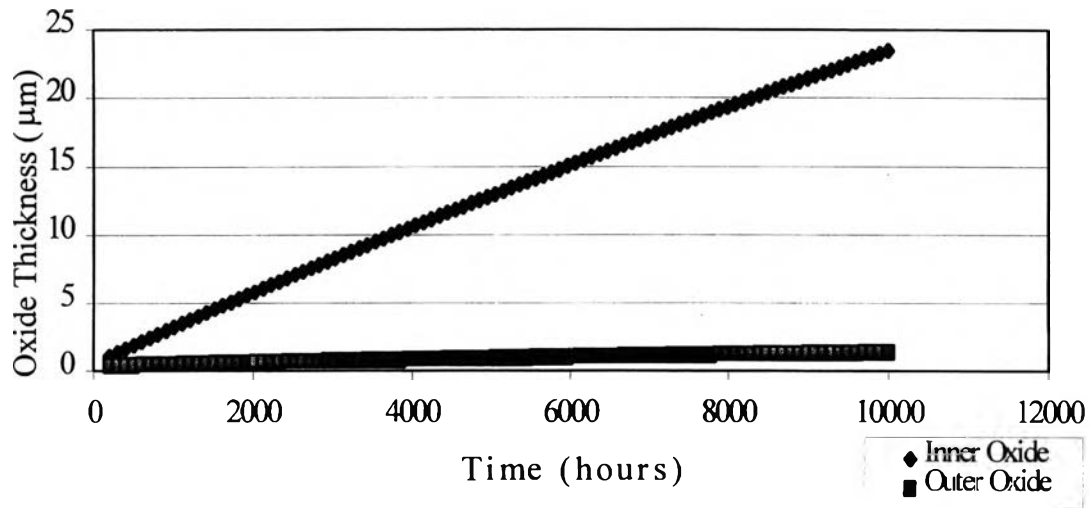### 4.2.2 The Effect of Mass Transfer Coefficient

The mass transfer coefficient for dissolved iron from the oxide/solution interface to the bulk solution is evaluated by Eq.3.37. To study the effect, the scaling factor for mass transfer coefficient was used. The result is shown in Table 4.6 and Figure 4.11.

**Table 4.6** The effect of mass transfer coefficient (h) on corrosion rate.

Scaling factor for h	Corrosion rate (μ m/yr)
0.001	13.93
0.005	18.58
0.01	19.97
0.05	25.08
0.1	40.40
0.5	85.91
1	108.66
5	126.31
10	102.63
20	101.23
50	126.77
100	135.60

For a low mass transfer coefficient, the resistance of mass loss is high. Therefore, the corrosion rate was low. The corrosion rate increased with mass transfer coefficient.

The oxide thickness affected by mass transfer coefficient is shown in Figures 4.11 and 4.12.

Figure 4.11 The oxide thickness profile with scaling factor for mass transfer coefficient was 0.01.
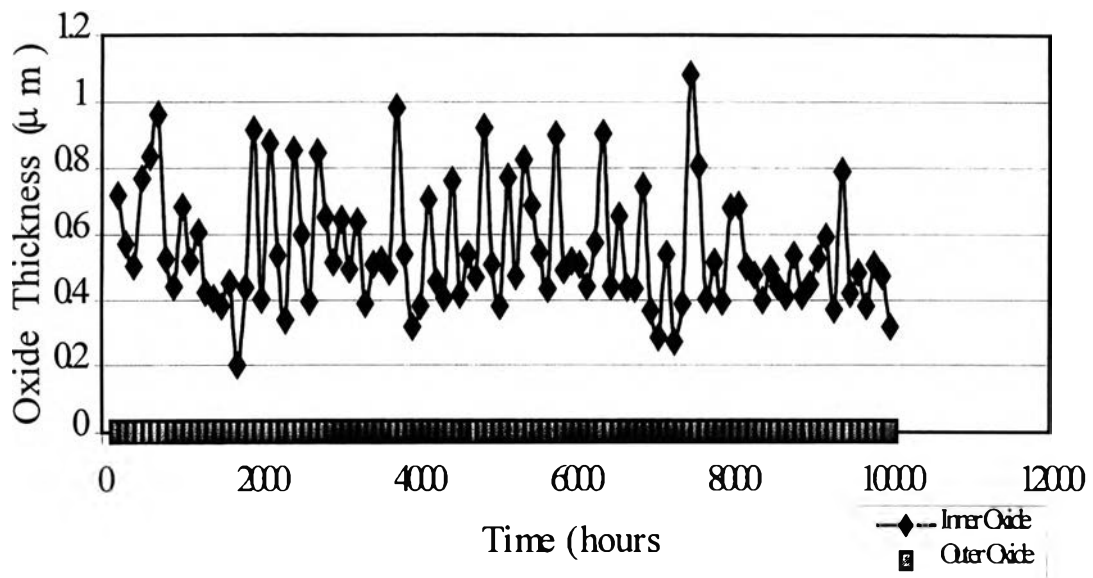
Figure 4.12 The oxide thickness profile with scaling factor for mass transfer coefficient was 1.

Figure 4.11 indicates that there is an inner and outer oxide layer. Plant data indicates no outer oxide layer on outer oxide thickness in the outlet feeders because of FAC effect. In this case, mass transfer coefficient was low, and allows accumulation of dissolved iron at the oxide surface. The concentration at the oxide surface increased to saturation, precipitation of oxide occurs. This does not occur in the plant from the observation. When

the mass transfer coefficient was increased in Figure 4.12, there was no outer oxide layer and the inner oxide thickness fluctuates due to the erosion and so does Figure 4.11 but on a different scale.

4.3 Application of the Model to the Tube Probe

There is the hypothesis that the dissolution rate constant changes with pH. The purpose of this study was to investigate this hypothesis. The effect of the spalling constant on oxide thickness is also discussed in this section. The corrosion rate of the tube probes for various pH values is presented in Table 4.7. The scaling factor for the dissolution rate constant (based on k_d at pH of 10.2) was used. The results from the prediction of corrosion rate for the tube probe at various pH values is presented in Table 4.8.

Table 4.7 The corrosion rate of tube probe (10m/s) from the experiment.

pH	Corrosion rate ($\mu m/yr$)
9.8	11.3
10.4	21.5
11.0	57
11.4	183
11.55	233

**Table 4.8** The scaling factor for kd at each pH and predicted corrosion rate of tube probe.

pH	Scaling factor for k_d	Predicted corrosion rate (μ m/yr)
9.8	0.000158	11.3
10.4	0.00064	21.5
11	14.5	57.5

From Table 4.8, it is observed that a low dissolution rate caused a low corrosion rate. At high pH, the dissolution rate should be high to obtain high corrosion rates corresponding with the experimental data. However, a high corrosion rate caused a corrosion rate oscillation because of the spalling phenomenon produced by erosion. Therefore, the corrosion rate at high pH could not be predicted reliably.

At low pH and low corrosion rate, the oxide layer was thick and constant, Figure 4.13. When the dissolution rate was increased, the spalling effect became important. Therefore, the fluctuation of oxide thickness occurred, Figure 4.14.

The effect of dissolution rate constant on the corrosion rate of both the wire probe and tube probe was similar. It can be concluded that the corrosion rate increases with an increase in the dissolution rate constant. A high dissolution rate causes high corrosion rate and a thin oxide layer.
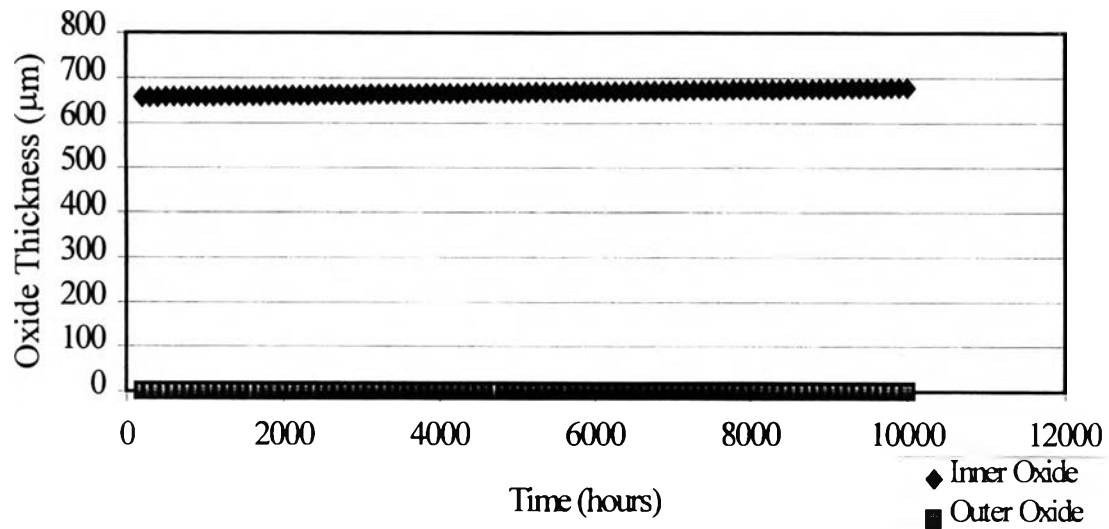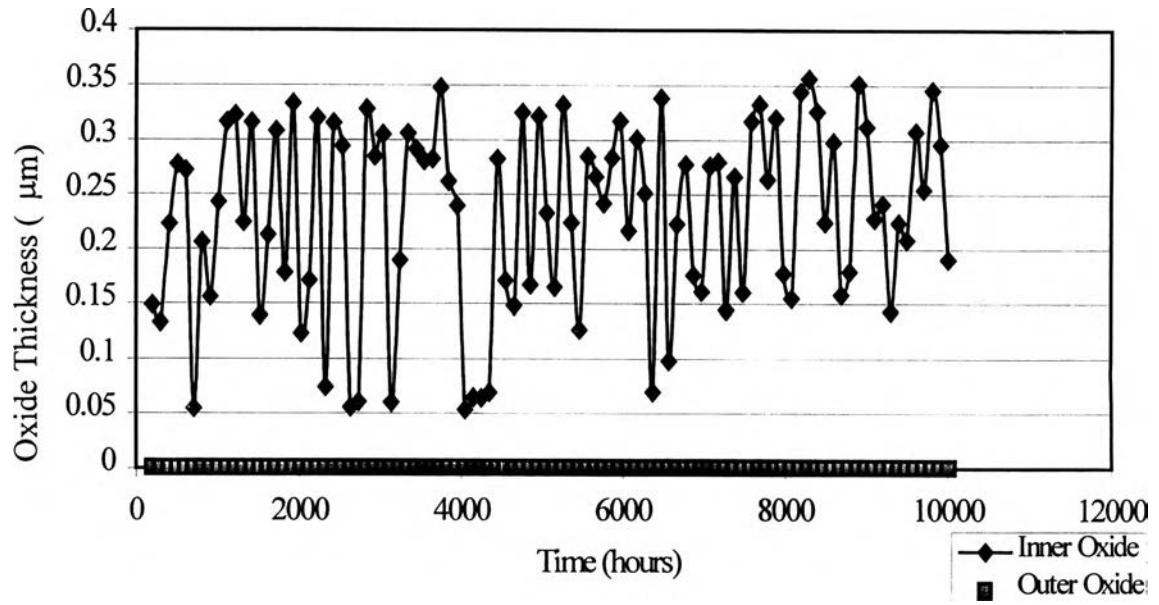
Figure 4.13 The oxide thickness profile of tube probe with scaling factor for k_d 0.00064.
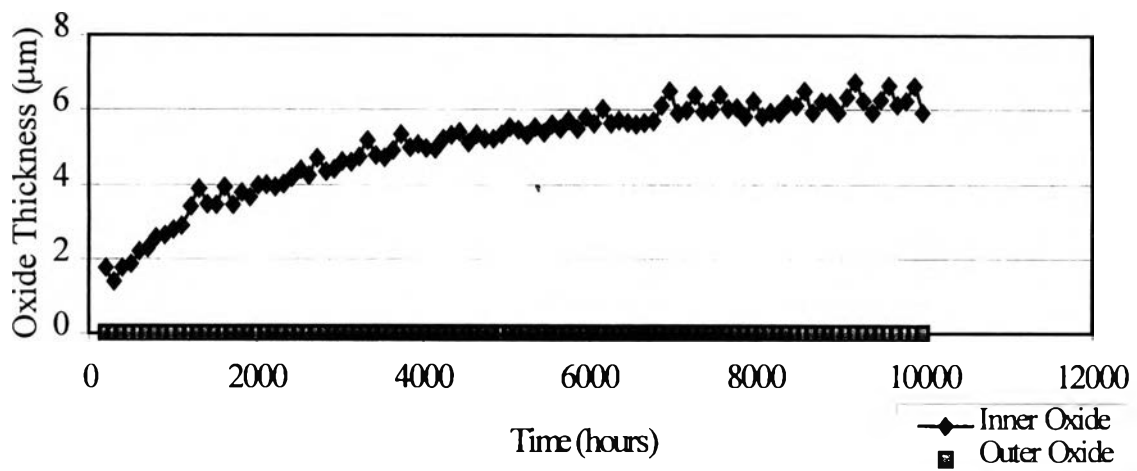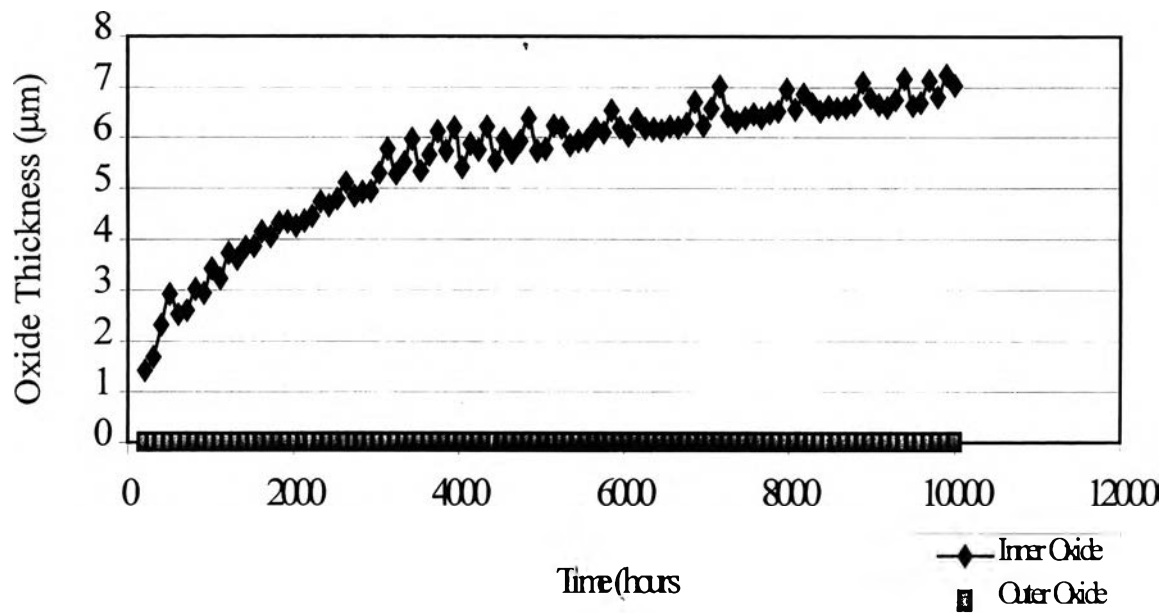

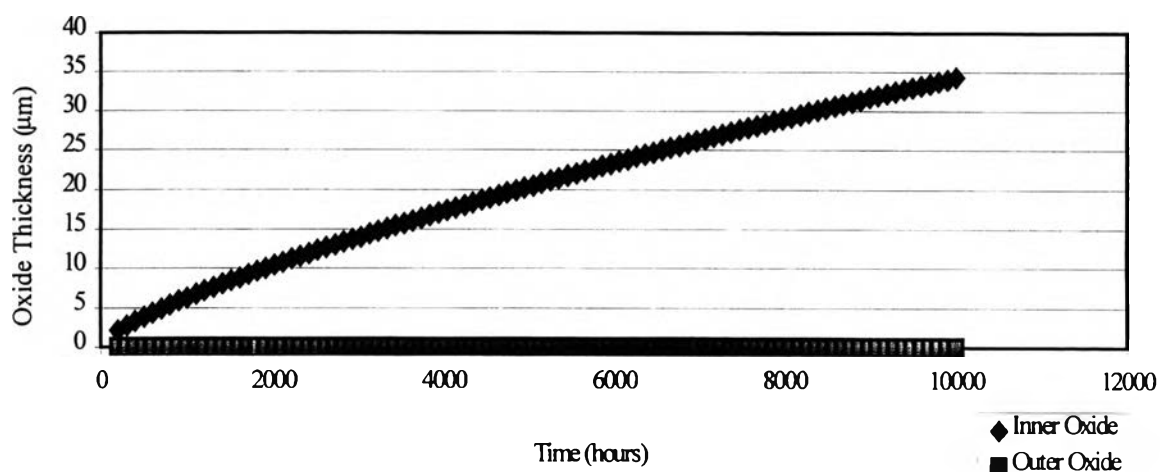**Figure 4.14** The oxide thickness profile of tube probe with scaling factor for k_d 1.

To study the effect of inner layer spalling constant, the scaling factor for the spalling constant (based on the spalling constant for feeder S08, the value was attached in appendix A) was used. The effect of spalling constant on oxide layer thickness is illustrated in Figures 4.15 to 4.17.

Figure 4.15 The oxide thickness profile of tube probe with scaling factor for spalling constant of 0.001.

Figure 4.16 The oxide thickness profile of tube probe with scaling factor for spalling constant of 0.1.

Figure 4.17 The oxide thickness profile of tube probe with scaling factor for spalling constant at 10.

Figures 4.15 to 4.17 demonstrate that if the spalling constant is low, the time for an erosion event is short. It is easy for a particle to spall off the surface. Therefore, the corrosion rate is high and the oxide layer is thin.

4.4 The Effect of Outer Oxide Layer on H_2 Diffusion

There was a hypothesis that outer oxide layer affects H2 diffusion through oxide film.

Table 4.9 The corrosion rate and oxide thickness of feeder S08 with and without outer layer effect on H_2 diffusion.

	Corrosion rate (μm/yr)	Oxide thickness (μm)
Without outer layer effect	110.2	0.76
With outer layer effect	109.5	0.80

The above table indicates that there is no significant effect of outer oxide layer on H_2 diffusion. The corrosion rates for both cases in Table 4.9 were similar. The expression for H_2 diffusion, Eq.3.28 can be rewritten as Eq.4.7.

$$5.66 \times 10^{-4} \frac{dm}{dt}(7.32 - \phi) = \frac{C_{w_{H_2}} - C_{ox_{H_2}}}{\frac{\tau}{D_{H_2}}\left(\frac{\delta_i}{\rho_{ox}\phi_i\left(1-\phi_i\right)}\right)} \qquad (4.7)$$

4.5 The Effect of Porosity on Corrosion Rate

Porosity is a property of the oxide that affects species transport through the oxide film. There are two layers of oxide which have different values of porosity. The outer layer commonly has a higher porosity than the inner layer.

This study was divided into three parts: 1)the effect of inner porosity, 2)the effect of outer porosity and 3)the effect of outer porosity and inner porosity.

To study the effect of inner porosity, the outer porosity was fixed at value of 0.3 and inner porosity was varied. The corrosion rate and oxide thickness of feeder S08 with 10000 exposure hours are presented in Table 4.10.

Table 4.10 Corrosion rate and oxide thickness when outer porosity was 0.3.

Inner porosity	Corrosion Rate (μm/yr)	Oxide thickness (μm)
0.003	13.9	6.5
0.015	27.4	2
0.03	44.6	0.7
0.1	109.1	0.15
0.3	105.9	0.02

It is observed that corrosion rate increased with inner porosity, while the oxide thickness decreased. A high inner porosity provides more space for the dissolved iron diffusing outwards. This increases the corrosion rate.

The effect of outer porosity was studied with inner porosity fixed at 0.1. The corrosion rate and oxide thickness of S08 within exposure time of 10000 hours are reported in Table 4.11.

Table 4.11 Corrosion rate and oxide thickness when inner porosity was 0.1.

Outer porosity	Corrosion Rate (μm/yr)	Oxide thickness (μm)
0.1	115.2	0.2
0.2	98.4	0.2
0.3	109.1	0.2
0.5	105.4	0.2
0.7	102.2	0.2
0.9	116.6	0.2

Table 4.11 indicates that the outer oxide layer did not affect the corrosion rate and the oxide layer thickness. Corrosion rates at different outer layer porosity were similar.

The effect of both inner and outer porosity was studied by fixing the ratio of outer porosity to inner porosity at 10. The results were shown in Table 4.12.

Table 4.12 Corrosion rate and oxide thickness when the ratio of outer porosity to inner porosity was 10.

| Outer porosity	Inner porosity	Corrosion rate (μ m/yr)	Oxide thickness (μm)
0.1	0.01	20.9	3.5
0.2	0.02	33.9	1.3
0.3	0.03	44.6	0.7
0.5	0.05	69.7	0.35
0.7	0.07	97.5	0.2
0.9	0.09	93.8	0.2

Table 4.12 indicates that the corrosion rate increased with the values of inner and outer porosity. However, the porosity of the inner oxide layer is controlling since the outer oxide layer is removed at high velocities.

4.6 Rationalizing Dissolution Rate Constant and Free Energy of Activation from Experimental Data

From the sensitivity analysis, it was found that the dissolution rate constant and the free energy of activation affected corrosion rate significantly. The dissolution rate constant is a function of temperature and pH.

From Figure 4.6, the relation between $\ln(k_d)$ and $1/T$ at pH of 10.2 is presented, and the proposed relation at pH of 11 with the assumption that the slope of this relation for various pHs should be the same. By this assumption,

dissolution rate constant at various pH values was determined and was used to predict corrosion rate for feeder S08, wire probe and tube probe. The predicted corrosion is displayed in Figure 4.18.
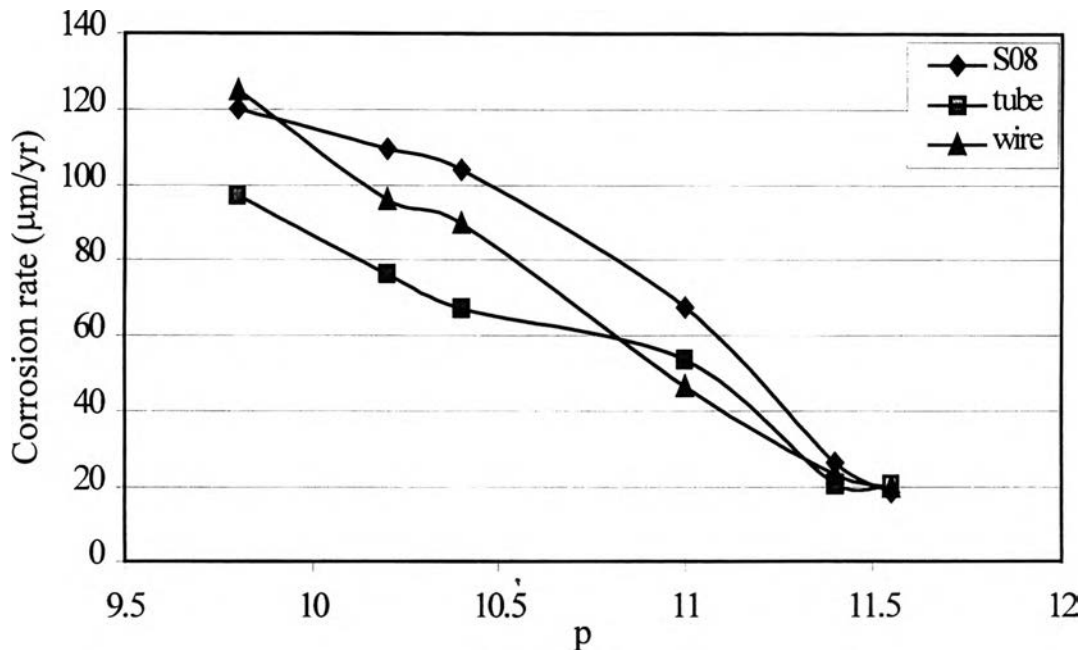
Figure 4.18 Corrosion rate of feederS08, wire and tube probes at various pH based on Figure 4.6.

The results from Figure 4.18 are not consistent with the results from the experiments, Table 4.2 and Table 4.7, for the wire probe and the tube probe. From the experiments, it was observed that corrosion rate increased with pH. Therefore the expression to determine dissolution rate constant at each pH was redetermined, Figure 4.19.
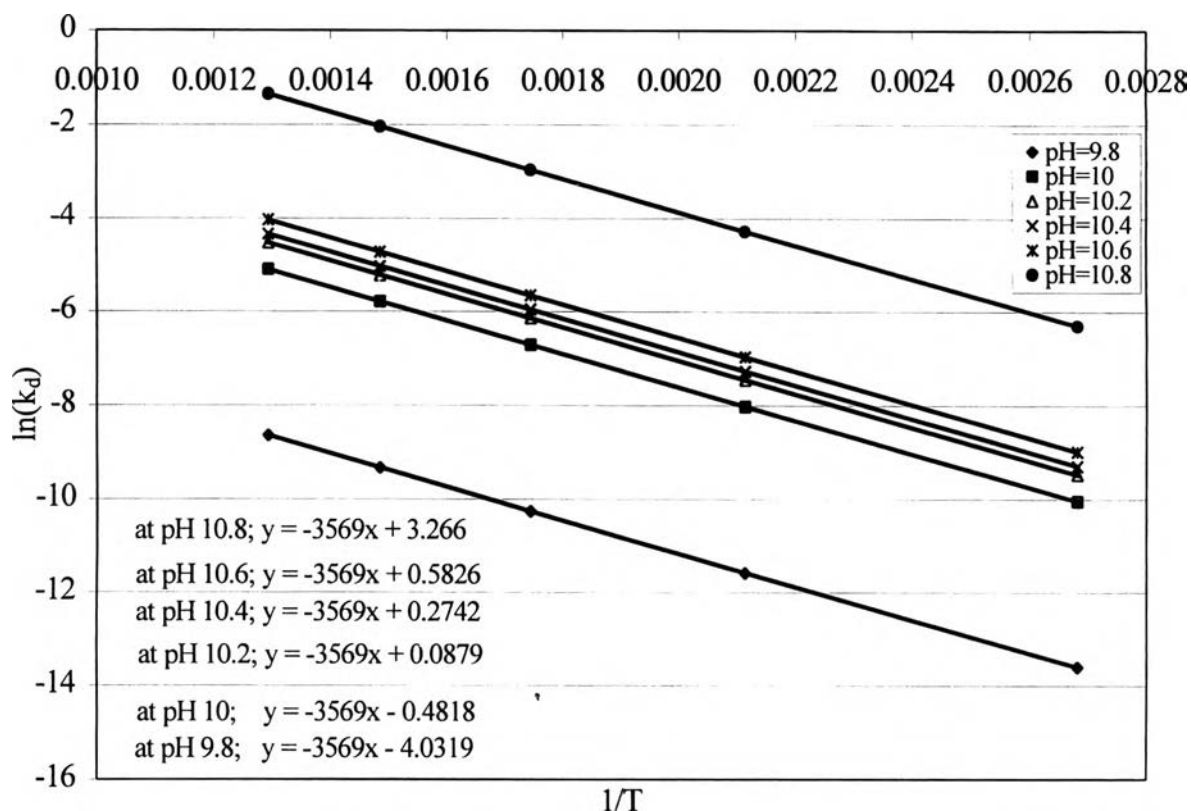
Figure 4.19 The expression for dissolution rate constant at various pH.

The free energy of activation was considered being important because it significantly affected corrosion rate, Table 4.1. Figure 2.9 illustrates the predominant species at different pH. These species may affect the free energy of activation for the reverse reaction of converting iron metal to dissolved iron. The reason for uses the activation energy of the reverse reaction for corrosion reaction is that this value is used to calculate the exchange current density when the reduction reaction is considered. Thus, the dissolved species are considered as reactants. Therefore, this free energy of activation depends

on pH. Actually, it depends on the species of dissolved iron that are present for the exchange current density equation.

Combining the change in dissolution rate constant and the activation energy, the free energy of activation was determined as a function of pH to allow the rate of corrosion to increase with pH.

$$\Delta G_1 = -12993 pH + 273938$$
$$R^2 = 0.9859$$
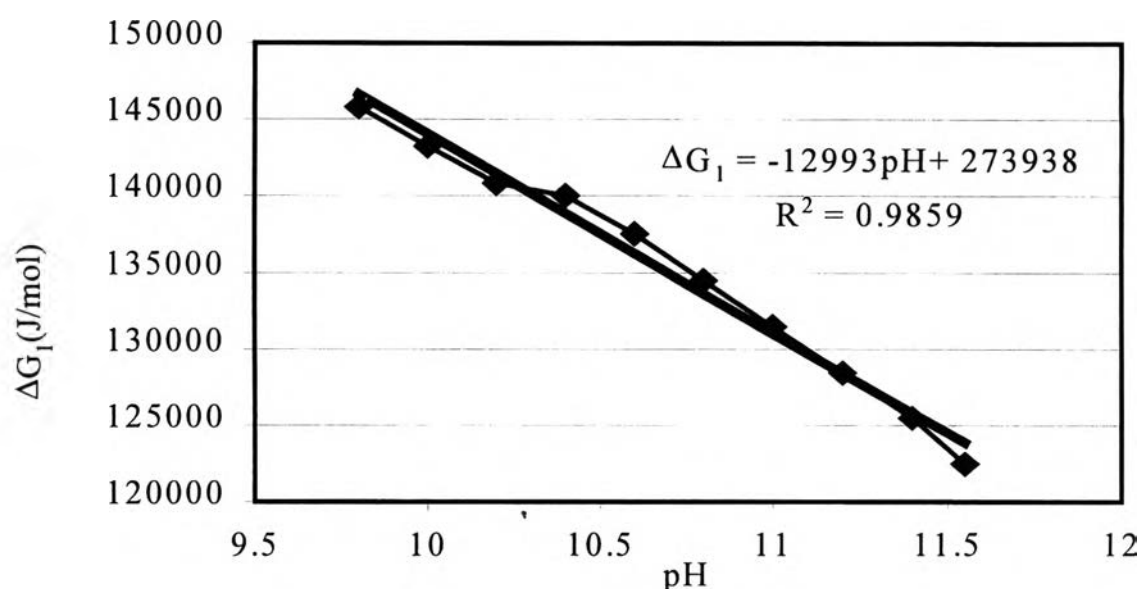
Figure 4.20 The relation between free energy of activation of reverse corrosion reaction and pH at 310°C.

From Figure 4.20, the free energy of activation of the reverse corrosion reaction can be determined as a function of pH at 310°C for this system by the expression 4.8.

$$\text{Free energy of activation} = -12993 pH + 273938 \qquad (4.8)$$

The dissolution rate constant was determined as a function of pH at 310°C as indicated in Figure 4.21. The dissolution rate constant was represented by a sixth order polynomial in terms of pH.
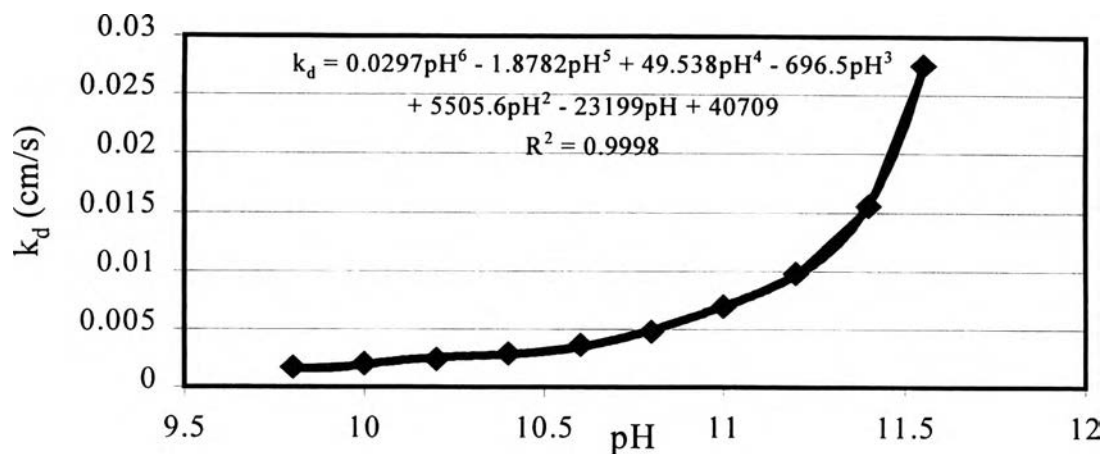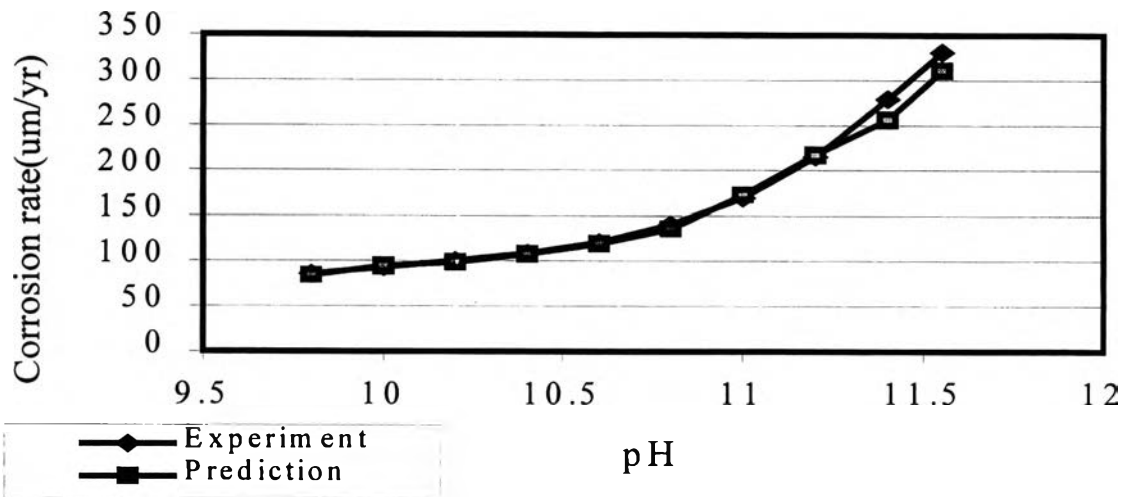
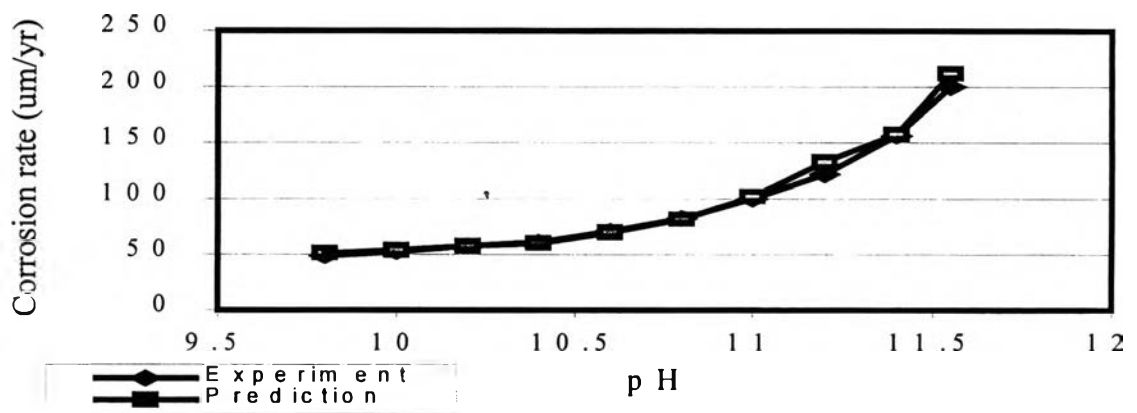**Figure 4.21** The relation between dissolution rate constant and pH at 310°C.

The dissolution rate constant can be determined at 310°C at various pH by Eq.4.9.

$$kd = 0.0297pH^6 - 1.8782pH^5 + 49.538pH^4 - 696.5pH^3 + 5505.6pH^2 - 23199pH + 40709$$

$$(4.9)$$

Both expressions for free energy of activation and dissolution rate constant were used to predict the corrosion rate and the oxide thickness of the wire and tube probes. The corrosion rates of the wire and tube probes are shown in Figures 4.22 and 4.23. The relations between oxide thickness and corrosion rate for wire probe and tube probe are displayed in Figures 4.24 and 4.25.
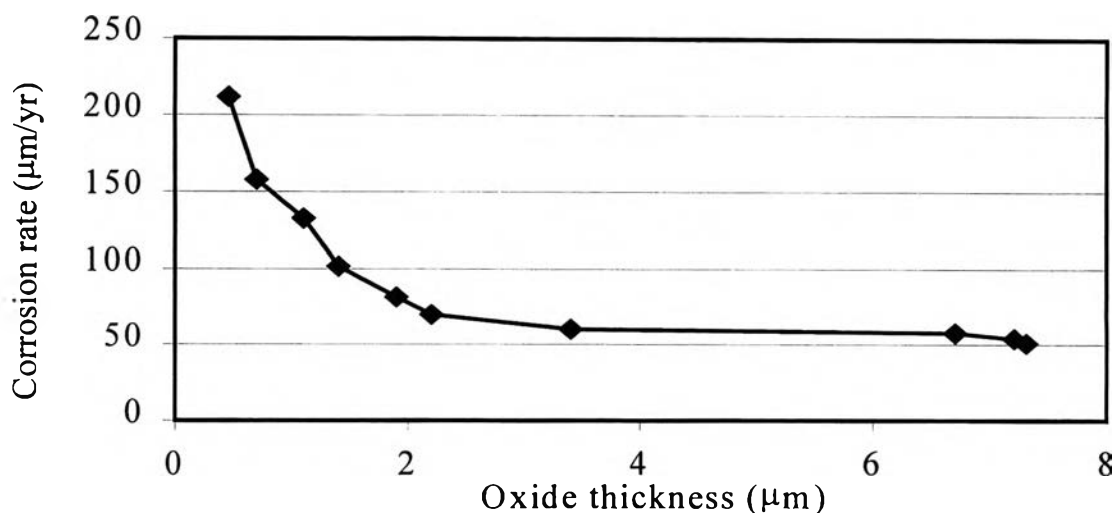
Figure 4.22 Corrosion rate of wire probe from experiment and prediction.

Figure 4.23 Corrosion rate of tube probe from experiment and prediction.
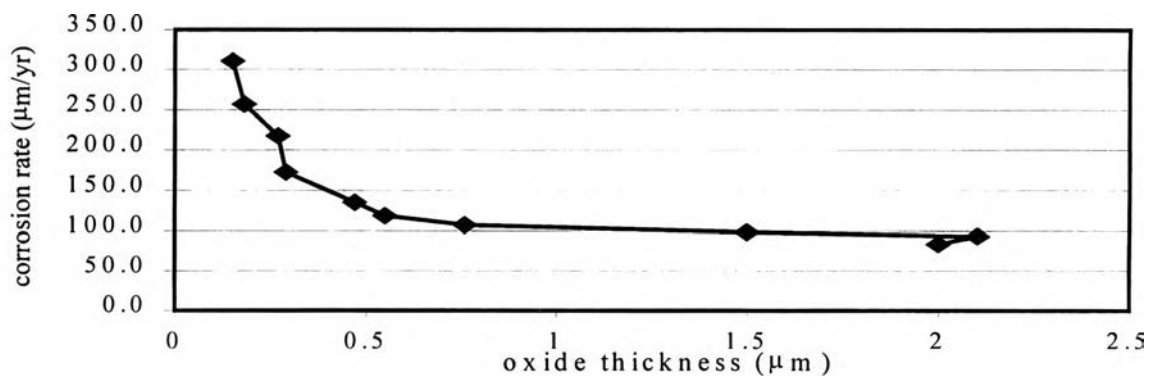
Figure 4.24 The relation between oxide thickness and corrosion rate of wire probe.

Figure 4.25 The relation between oxide thickness and corrosion rate of tube probe.

The corrosion rates from the experiment and predicted values are similar, Figures 4.22 and 4.23. Figures 4.24 and 4.25 give the relation between oxide thickness and corrosion rate for wire probe and tube probe. The expressions for determining the activation energy and the dissolution rate constant yield corrosion rates which agree with experimental values. However, additional data are required to substantiate these results over a wider range of conditions.

Because of electrochemical effects that are complicated concerning this model, the simpler model was proposed. The simpler model is based on reaction rate and mass transfer of dissolved iron. The simpler model is described in the Appendix E. The simpler model is interesting and can be developed in further.